Simulation Standard

TCAD Driven CAD

A Journal for Process and Device Engineers

New, Fast Numerical Algorithm for Diffusion Modeling Implemented in ATHENA Version 5.0

Fast Diffusion Module

A new diffusion algorithm based on a Galerkin method with linear finite elements, an extremely fast sparse matrix solver, and object oriented physical modeling is one of the new features implemented in ***ATHENA*** version 5.0. This module is an alternative to the existing code, thus providing the user with a choice between using the old diffusion module and the new algorithms.

The Implicit Linear Finite Element Method (ILFEM) module is available for diffusion and oxidation steps. Switching between the two modules is done using a METHOD statement in the input file, giving the user a flexible choice between numerics for each individual diffusion run.

The advantages in adding a new diffusion module to ***ATHENA*** are:

- The spatial discretization scheme employed in ***SSuprem4*** causes a slow-down during simulations on grids with poor geometry. Due to the inability of the first order finite volume method to deal with triangles with large aspect ratios. An excessive amount of time is spent doing Lawson flipping, whenever skinny triangles start to accumulate at the moving *Si-SiO$_2$* interface during oxidation.
- The existing diffusion code may run into convergence problems during simulations on structures that involve polysilicon interfaces.
- The methods for linear system solving in ***SSuprem4*** were inherited from the original Stanford SUPREM-IV[1]. There are not fully up to date with most recent progress within the field. For optimal efficiency, most contemporary simulators use iterative sparse linear solvers, whenever possible[1].
- When a high concentration of <311> interstitial clusters are present in the structure there may be numerical problems.

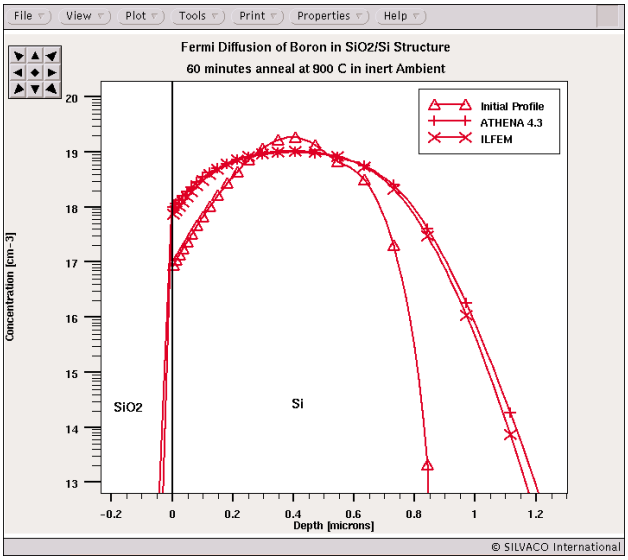

Figure 1. Boron anneal using ILFEM and ATHENA.

- Improvement modeling of interstitial traps, as described by P. Griffin [2].
- The code on which the original diffusion simulator is based, was created before object-oriented programming paradigms and tools to support it became prevalent. When programs based on procedural programming grow large, they tend to become unmanageable, thus degrading both maintainability as well as extendibility. For rapid implementation/testing of new physical models, well organized base code is of paramount importance.

Continued on page 2....

INSIDE

SILVACO INTERNATIONAL

In the following sections, the new module will be described in more detail, especially how it addresses some of the above mentioned problems in ***SSuprem4***.

The Physics

It may be shown that it is not energetically favorable for an impurity atom to migrate on its own in a semiconductor lattice. Overcoming the large Coulomb repulsion in the diffusion saddle point makes this mechanism rather prohibitive, so dopant diffusion is believed to predominantly take place through interaction with point defects[3]. A dopant atom can form a pair with either an empty lattice site (a vacancy, V) or a substrate atom sitting between regular lattice sites (a self interstitial, I), and the pair as a whole then diffuses through a number of inversion cycles. The set of reaction-diffusion equations solved in ***ATHENA*** is based on such a dopant / point-defect pair diffusion mechanism[1]. In the following we ignore the fact that dopant-defect pairs can exist in different charge states.

Dopants:

The continuity equation for dopants is

where C_A designates the total concentration of dopant A

$$\frac{\partial C_A}{\partial t} = \sum_{X=I,V} \nabla \cdot J_{AX} \qquad (1)$$

and J_{AX} is the pair flux. Notice that this expression explicitly states that dopant atoms can only move via the pair mechanism. The flux expression for dopants is

$$J_{AX} = \left(\frac{C_x}{C_x^*} \cdot D_{AX}\right) C_{A+} \nabla ln \left(C_{A+} \frac{C_x}{C_x^*} \left(\frac{n}{n_i}\right)^z\right) \qquad (2)$$

where D_{AX} is the pair diffusivity, C_{A+} is the electrically active dopant concentration, C^*_X designates the equilibrium defect concentration, and Z is the dopant charge number (+1 for donors and -1 for acceptors). The dopant flux expression (2) incorporates contributions from both the dopant gradient, a supersaturation of point defects, as well as an internal electric field. The pair diffusivity is actually a composite entity, taking into account the distribution of pairs over different charge states as well as fermi level enhancement effects, according to the following expression

$$D_{AX}(n,T) = \sum_{c=0,\pm1,\pm2} D_{AX}^{-c}(T) \left(\frac{n}{n_i}\right)^c \qquad (3)$$

where *c* is the charge state, *n* and *ni* are the actual and intrinsic carrier concentration, respectively, and the temperature dependency of the intrinsic pair diffusivity, D_{AX}^{-c} is given by an Arrhenius expression,

$$D_{AX}^{-c} = prf * exp\left(\frac{-E_a}{k_B T}\right) \qquad (4)$$

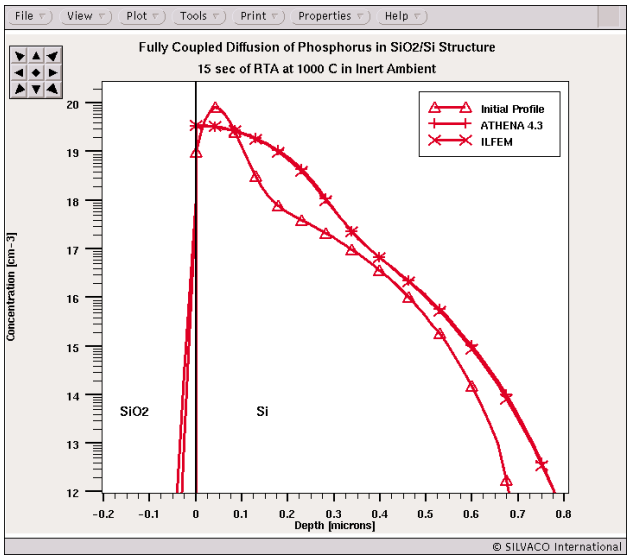

Figure 2. Fully coupled phosphorus diffusion using ILFEM.

In the *fermi model*, vacancies and self interstitials are assumed to be in thermodynamical equilibrium, and the defect supersaturation ratio $\frac{C_x}{C_x^*}$ becomes unity in (2).

Point Defects

Due to implantation damage and injection during oxidation and nitridation, the point defect populations can in general *not* be assumed to be in equilibrium, for which reason explicit representation and evolution of these species is needed.The continuity equations for vacancies and interstitials are

$$\frac{\partial C_V}{\partial t} = \nabla \cdot (-J_V - J_{AV}) - R, \qquad (5)$$

$$\frac{\partial C_I}{\partial t} = \nabla \cdot (-J_I - J_{AI}) - R \qquad (6)$$

where *R* is a recombination term that accounts for the creation / annihilation of interstitial-vacancy pairs in the semiconductor bulk,

$$R = K_R (C_V C_I - C_V^* C_I^*) \qquad (7)$$

with K_R a rate constant. The point defect flux expressions are given by

$$-J_V = D_V C_V^* \nabla\left(\frac{C_V}{C_V^*}\right), \quad -J_I = D_I C_I^* \nabla\left(\frac{C_I}{C_I^*}\right) \qquad (8)$$

which correctly accounts for the effect of an electric field on the charged portion of the defects (the defect equilibrium concentrations, C^*_V and C^*_I, are fermi level dependent).For the sake of brevity, neither boundary conditions nor interactions with interstitial traps, <311> clusters, nor dislocation loops have been mentioned.

The presence of the pair fluxes, J_{AV} and J_{AI}, in (5) and (6) represent the contribution from paired defects to the total time rate of change of the defect populations, and establishes a two-way coupling between the diffusion of dopants and point-defects. Therefore, the three-species model defined by eqs. (1), (5), and (6) is called the *fully coupled* diffusion model. For simplification, summation over all present dopants and charge states has been omitted. In reality, there should be a pair flux correction term from every combination of these degrees of freedom. Under circumstances where the pair fluxes become very small in comparison to the fluxes of free point defects, the fully coupled correction terms can be omitted altogether. This is equivalent to zero binding between dopants and defects, and is called the *two-dimensional* diffusion model.

The system of coupled partial differential equations defined by the the equations (1), (5) and (6) is both non-linear and stiff, so special attention is required in the numerical treatment. Particularly, the time discretization method used for integrating a stiff PDE system must be robust in order to avoid numerical instability[2]. The original diffusion module uses a composite trapezoidal second order backward differential rule (TR-BDF2) for the time integration, while ILFEM uses a backward euler one step rule. The TR-BDF2 [4] method has a smaller local truncation error (third order in time) than backward euler (second order in time), which, on the other hand, is easier to implement. Both methods, however, do satisfy the stability requirements needed to deal with stiff problems.

The segregation of dopant impurities across interfaces is modeled by means of a simple first order kinetic model

$$J = h_{12}\left(\frac{C}{M_{12}} - C_2\right) \qquad (9)$$

where C_1 and C_2 are the particle concentrations in the immediate vicinity of the interface, h_{12} is the *transport velocity*, and M_{12} is the segregation coefficient, defined as the ratio between solubilities of the dopant in the two materials sharing the interface. For the new diffusion module, h_{12} has been set artificially large, thus forcing the dopant to instant equilibration on the interface. This *penalty method*, of course, does not lend itself to the modeling of transient segregation phenomena, but, on the other hand, is an efficient method for the damping out of numerical oscillations that tend to originate on the interface where the dopant profile is discontinuous.

Spatial Discretization

The finite volume method, runs into difficulties when obtuse or skinny triangles are present in the grid. The method depends on the correct calculation of Voronoid cell areas as well as coupling coefficients, both of which fail in the partitioning of an obtuse triangle. This causes numerical havoc, inducing such unphysical effects as reversing the direction of diffusion flow through cells or distortion of the flux. To prevent the forming of triangles of bad aspect ratios during oxidizing runs, the grid topography has to be constantly monitored throughout the simulation, and when a bad triangle is encountered, a Lawson flip of edges is required. This extra overhead, not surprisingly, may cripple the performance during simulations of heat cycles in oxidizing ambients.

A standard Galerkin linear finite element methods has been chosen for the ILFEM diffusion module. This method is of second order precision in the spatial variables, uses linear test functions, and is well suited for irregularly shaped geometries. Most important of all, though, is the fact that it is totally immune to the pathological grid effects mentioned above.

Iterative Sparse Linear System Solver

The ILFEM diffusion module uses a very fast iterative sparse linear solver that employs domain decomposition preconditioning. A significant performance increase in linear solving has been observed in benchmark tests. The performance gain, though, depends on various factors such as the size of the grid, and the condition number and sparsity structure of the stiffness matrix. The relative performance is best for large, symmetrical matrices.

Object Oriented Physical Modeling

The new module is a total rewrite of the diffusion solver, using object-oriented design from the bottom-up. The objective has been to both reproduce ***SSuprem4***'s basic three diffusion models as well as to provide a solid frame work for future implementation of new physical models that lends itself to rapid development,

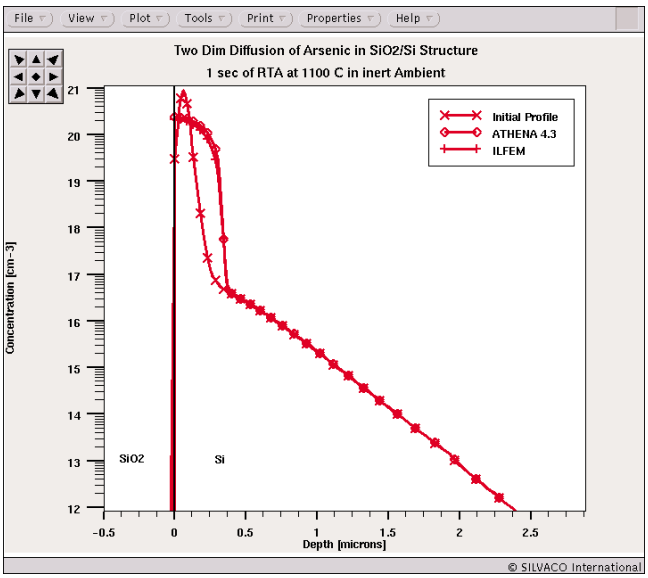

Figure 3. Defect enhanced diffusion of arsenic using ILFEM enhanced.

robust code, and easy verification and validation.

The design incorporates the following features

- Models implemented as a C++ class hierarchy
- Dynamical creation of physical model objects (:created when needed)
- Smart model switching
- Dynamical creation of FEM matrix generators
- Localization of all model parameter information
- Logging of all used model parameters for debugging and control
- Extensive use of polymorphism
- Easy introduction of new materials and impurities through localization of control logic
- Separation of models, grid information, and numerics

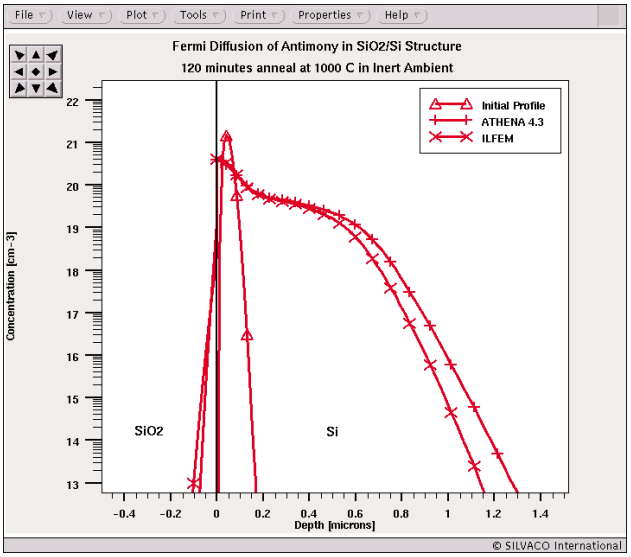

FIgure 4. High temperature antimony diffusion in ILFEM.

Diffusion Modeling

From a modeling perspective the goal of the new diffusion module, as implemented in the 1999 ***ATHENA*** release, has been to reproduce ***SSuprem4*** except in situations where the diffusion modeling of the latter is either wrong or artificial. Such exceptions include

- ***SSuprem4***'s unphysical pile-up of dopants at oxide/gas interfaces. Using the new diffusion module, the dopant profile will instead make a dip near the oxide/gas interface because of dopant loss to the ambient
- A correction of the implementation of the fermi diffusion model for indium, which was flawed in ***SSuprem4***. is also included
- ***SSuprem4*** modeling of the interstitial trap reaction, has much too high trap reaction rate. The rate has been changed to a more physically appropriate value, resulting in a more smooth fall-off of the edge of the interstitial profile during coupled diffusion.

For the current release four models have been ported to ILFEM: The fermi model, the two dimensional mode, the fully coupled model, and finally the high concentration fully coupled model as formulated by S. Crowder [5].

The following illustrations show 1D diffusion profiles for four commonly used dopants in different physical scenarios (dose, implant energy, diffusion model, anneal temperature). Each graph contains an initial profile and the results obtained through ***ATHENA*** 4.3 and ILFEM, respectively. All examples employ a simple SiO2/Si structure in order to model the diffusion of the dopant in silicon as well as its segregation across a silicon/oxide interface. For each case a 0.5 micron oxide layer was deposited after dopant implant, using 20 grid divisions. Notice that all profiles are displayed in a semi logarithmic plot.

Figure 1 shows a simulation of a one hour fermi diffusion at 900 C of a medium dose, high energy boron implant (5e14 cm-2, 80 keV). Since n_i, the intrinsic carrier concentration is about 4e18 cm-3 at this temperature, the doping is extrinsic between 0.2 microns and 0.62 microns, for which reason some fermi level enhanced diffusion should be expected. The agreement between ***ATHENA*** 4.3 and ILFEM is seen to be overall good, ***ATHENA*** 4.3 being slightly more diffusive in the tail region of the profile. There also seems to be good consistency with respect to the amount of segregation of boron into the oxide layer. One should bear in mind, though, that ILFEM employs infinite high transport velocities across all interfaces, so during the time of transient segregation the profiles should be expected to differ slightly in the oxide.

Figure 2 shows a fifteen second fully coupled diffusion at 1000 C of a medium dose phosphorus implant (5e14 cm-2, 35 keV). The implant model used was dual pearson with a damage factor of 0.1. Since the intrinsic carrier concentration is about 1.0e19 cm-3 at 1000 C, the joint effects of fermi level enhancement and TED (Transient Enhanced Diffusion) are to be expected in the diffused phosphorus profile. The agreement between ILFEM and ***ATHENA*** 4.3 is seen to be excellent both below as well as above the characteristic phosphorus kink.

Figure 3 shows the simulation of a one second 1100 C RTA profile of a high dose arsenic implant (5e15 cm-2, 80 keV), using the two.dim diffusion model. The intrinsic carrier concentration is about 1.2e19 cm-3 at 1100 C, so the silicon less than 0.3 microns from the SiO2/Si interface is highly extrinsic. Apart from a slight deviation in the peak region of the arsenic profile which might be due to a minor difference in the implementation of the AsV clustering model, the agreement between ***ATHENA*** 4.3 and ILFEM is again good.

Figure 4 shows a two hour fermi diffusion at 1100 C of a high dose antimony implant (5e15 cm-2, 80 keV). Again the interface region of the semiconductor is highly extrinsic, so fermi level enhancement is expected. Due to the low solid solubility of substitutional antimony in silicon, a peak of clustered / precipitated antimony can be observed near the silicon / oxide interface. While the agreement between ***ATHENA*** 4.3 and ILFEM is still good in the dopant peak region, there is a slight deviation in the tail region as well as in the oxide.

Benchmarks Tests

Four different benchmark tests have been carried out in order to compare the performances of the two diffusion simulators. The first test involves an RTA activation of a high dose source-drain implant, the second test consists of the process part of the formation of a vertical DMOS device the third test is 420 minutes of fermi diffusion on a power device, and finally the fourth test simulates one second of fully coupled diffusion of a 1.0e15 cm-2 dose arsenic implant with high implant damage. All simulations were executed on a Sun UltraSPARC-IIi 300MHz workstation.

The results are presented in Table 1.

This relatively small collection of benchmarks should not be interpreted as a decisive proof that the original code is always inefficient, but more as an indication of what kind of gain may be expected in situations where ***SSuprem4*** seems to have performance problems, namely in the case of coupled diffusion on medium size structures involving poly, coupled diffusion on structures with large implantation damage, and ultimately for all diffusion simulations on large 2D structures.

Prospects for the Future

For the release after 5.0, the following additional features are planned

- Rapid Implementation of state-of-the-art reaction-diffusion models
- Updating of all model parameters through assimilation of newest scientific results
- Addition of more materials and impurities (GaAs, SiGe, e.t.c.).
- Fast model prototyping by means of fast C-interpreter
- Additional grid generators
- Additional matrix generators.
- Database management of all model parameters

Footnotes

1. The applicability of such solvers depends intimately on sparsity structure, condition number, and other characteristics of the linear system.
2. Among numericists, the capability of a time integration method to deal with systems of stiff PDE's is called *L-stability*.

References

[1] M.E. Law, ``Two Dimensional Numerical Simulation of Dopant Diffusion in Silicon'', PhD Thesis, Department of Electrical Engineering, Stanford University, Jan. 1988.

[2] P.B. Griffin and J.D. Plummer, ``Process Physics Determining 2-D Impurity Profiles in VLSI Devices'', International Electron Devices Meeting, p.522, Los Angeles, Dec. 1986.

[3] R.B. Fair, (ed. F.F.Y. Wang), ``Concentration Profiles of Diffused Dopants in Silicon'', \textit{Impurity Doping Process in Silicon}, North Holland, New York, 1981

[4] R.E.Bank, W.M.Coughran, W.Fichtner, E.H.Grosse, D.J.Rose, and R.K.Smith, ``Transient Simulation of Silicon Devices and Circuits'', \textit{IEEE Trans. Electron Devices}, vol. ED-32, p.1992, Oct. 1985

[5] S. Crowder, ``Processing Physics in SOI Material'', PhD Dissertation, Department of Electrical Engineering, Stanford University, 1995

Example	Model	Nodes	ATHENA 4.3	ILFEM	Speedup Factor
MOSFET	two.dim	2829	583s	240s	2.43
Vertical DMOS	fermi	458	119s	99s	1.2
Power Device	fermi	8250	318s	85s	3.74
Arsenic Activation	full.cpl	672	429s	68s	6.31

Table 1.CPU time comparison showing ILFEM speedup factor.

Mixed Circuit Device Simulation of Single Event Upset in a Memory Cell

Introduction

This article presents Single Event Upset (SEU) simulation of a SRAM cell using ***MixedMode3D***. ***MixedMode3D*** provides the capability to simultaneously perform circuit simulation coupled with three-dimensional device simulation. This allows one to examine the internal operation of a three-dimensional numerically simulated device and predict the response of the attached circuit in a self consistent manner.

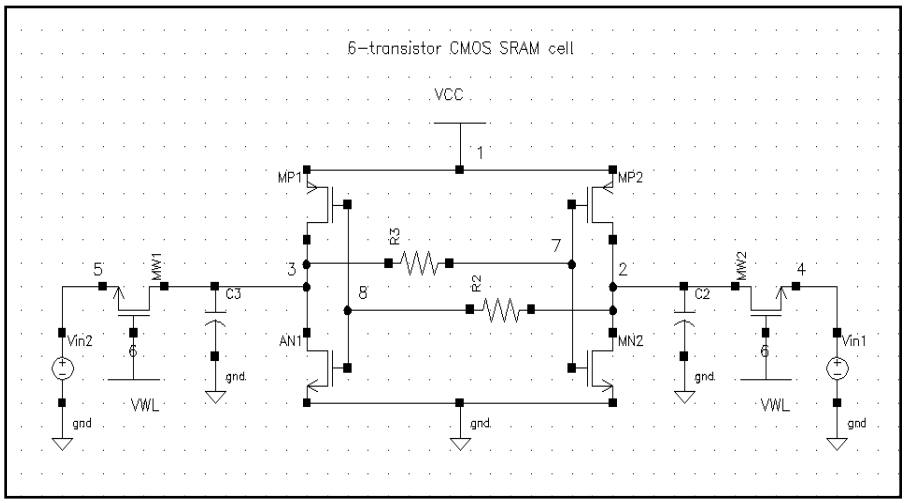

Figure 1. Schematic Diagram of a Six Transistor SRAM Cell

When an ionized particle interacts with a semiconductor, electron-hole pairs are generated along the path of the incident particle [1]. These generated electron-hole pairs can be transported through the semiconductor by drift and diffusion processes, which ultimately can affect transient device currents. Under certain biasing conditions the transient currents can alter the previously stored state of the circuit, causing an error in the data stored in the circuit. This phenomenon is generally referred to as Single Event Upset (SEU) [2].

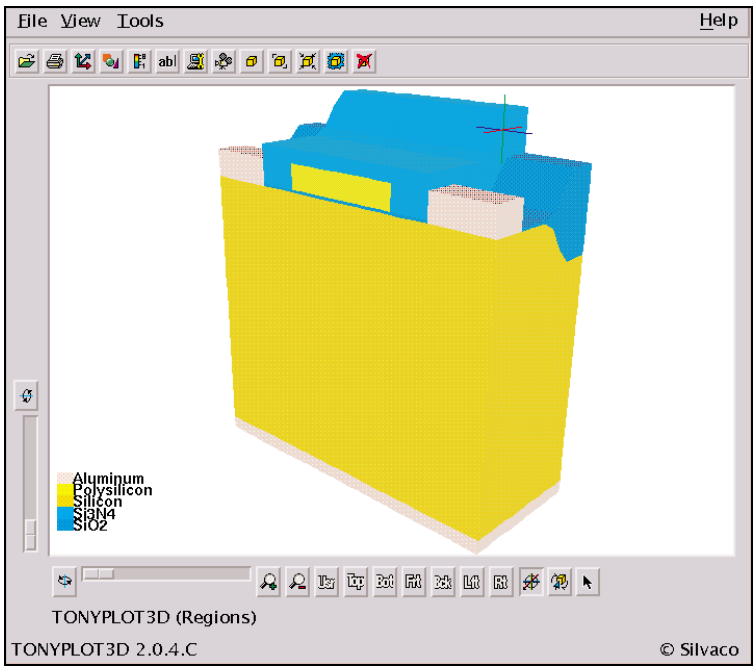

Figure 2. Three-Dimensional NMOSFET Structure Created With ***DevEdit3D***.

Simulation Results

Inputs to ***MixedMode3D*** are defined in a text file and include the following information: netlist representation of the circuit, model specifications for the numerically simulated device, SPICE model specifications and parameters, SEU strike definition, and biasing conditions for DC and transient analysis.

A schematic diagram of a six transistor SRAM cell is shown in Figure 1. Five of the six devices shown are simulated with appropriate SPICE models to describe their electrical characteristics. The sixth transistor (AN1) is a three-dimensional numerically simulated NMOSFET. The electrical characteristics of device AN1 are simulated by solving Poisson's equation and current continuity equations at discrete 3D grid points.

Using ***DevEdit3D*** a three-dimensional NMOSFET (Figure 2) is created by defining the material regions, doping concentrations, and electrodes. After building a 3D mesh for

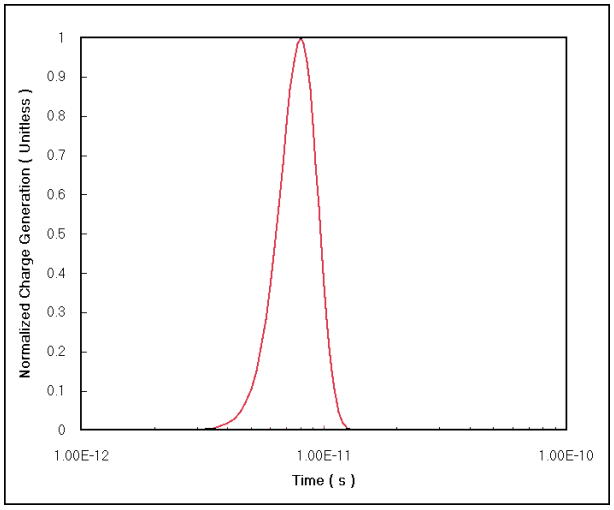

Figure 3. Single Event Upset Normalized Charge Generation Versus Time

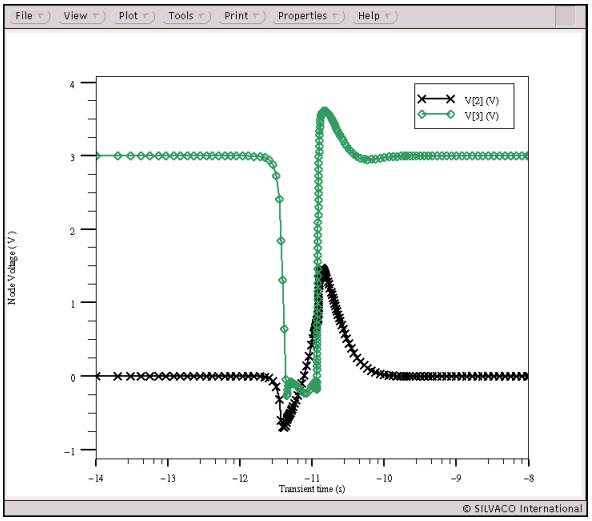

Figure 5. Internal SRAM storage Node Voltage Versus Time.

the NMOSFET, the information is stored as a structure file for use in the ***MixedMode3D*** simulation.

The DC biasing of the SRAM circuit sets the word line (node six) to zero volts, and nodes three (drain of AN1) and two, to three and zero volts, respectively. This biasing scheme sets the initial condition of the circuit for subsequent transient analysis.

The description of the SEU strike is specified on the SINGLEEVENTUPSET statement. Entry and exit locations of the SEU particle are defined using (x,y,z) coordinates for each point. The single event upset track is assumed to be cylindrically shaped with the cylinder's center located along the line defined by the entry and exit locations. Electron-hole pair generation rates along the SEU track can be specified as a function of the radius of the cylinder, the length of the track, and the duration of the charge generation pulse [3]. Figure 3 shows the normalized charge generation pulse used in the simulation. The maximum charge occurs at 8 picoseconds and decreases in a Gaussian fashion. Figure 4 shows the electron concentration distribution in the device resulting from a SEU strike directed from the upper left-hand corner to the lower right-hand corner.

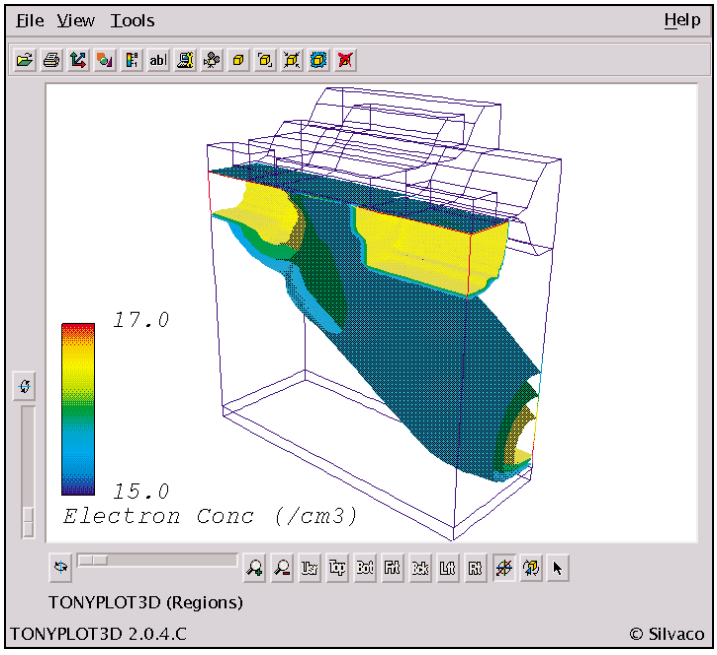

Figure 4. Three-Dimensional NMOSFET Structure Showing Location of Single Event Upset Strike.

Transient analysis is carried out for ten nanoseconds with an initial time step of ten femtoseconds. Figure 5 shows the resulting node voltages during the transient analysis. The initial voltage on the drain of AN1 (node three) is three volts. As the SEU strike enters the NMOSFET, electron-hole pairs are created and the voltage at the drain of AN1 (node three) is reduced to approximately zero volts. This low voltage state on node three causes transistor MP2 to begin conducting, and the voltage at the drain of MP2 (node two) begins to increase. When the external source of electron-hole pairs is removed, the system recovers and the initial potential values are restored at nodes two and three. If the duration of the strike had been longer, a complete reversal in the state of nodes 2 and 3 would occur.

Figure 6 shows isosurfaces of electron concentration in the three-dimensional NMOSFET at two times during the transient analysis. Figure 6(a) shows the electron concentration before the SEU

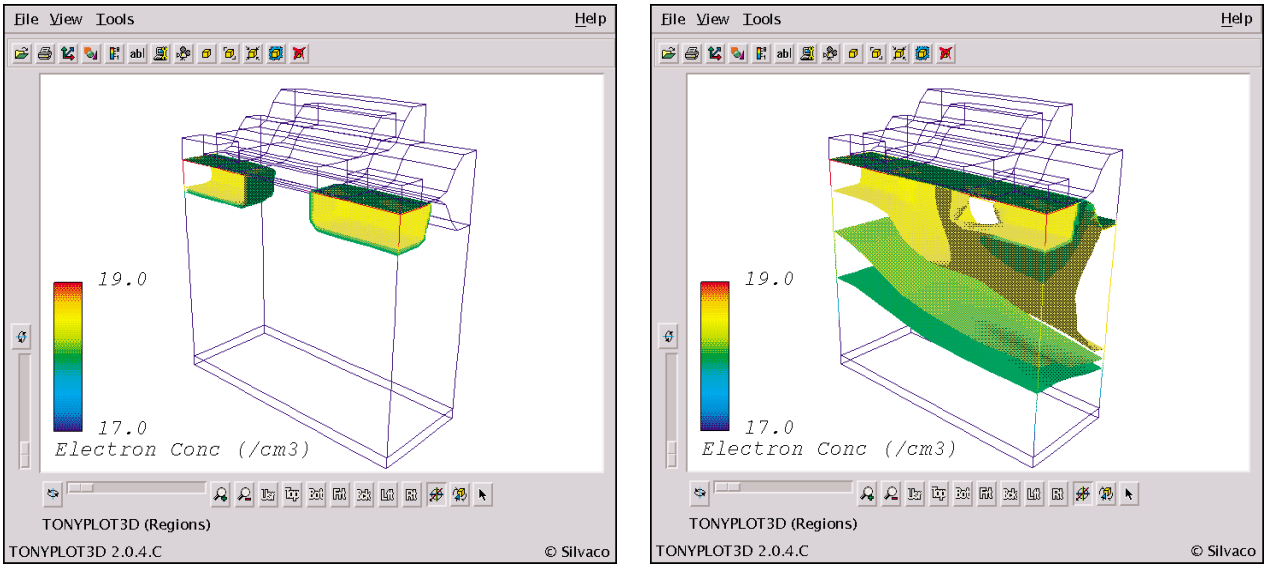

Figure 6. Electron Concentration Isosurfaces (a) Before SEU Strike (b) During SEU Strike When Electron-Hole Pair Generation is Near a Maximum

event. Figure 5(b) shows electron concentration isosurfaces when the electron-hole pair generation from the SEU strike is near a maximum (approximately 8 picoseconds). The corresponding potential distributions for these two cases are shown in Figure 7.

Summary

Simulation of Single Event Upset of an SRAM cell with ***MixedMode3D*** was presented. Predicting circuit responses due to ionized particle interactions with semiconductor devices and visualizing the internal operation of a three-dimensional device under these conditions are valuable tools for device design and circuit testing.

References

[1] IEEE Nuclear and Space Radiation Effects Conference Short Course, Chapter 3, Snowbird, Utah, July, 19, 1993.

[2] G. C. Messenger and Milton S. Ash, "The Effects of Radiation on Electronic Systems," Chapter 8, Van Nostrand Reinhold, New York, NY, 1992.

[3] ATLAS Users Manual

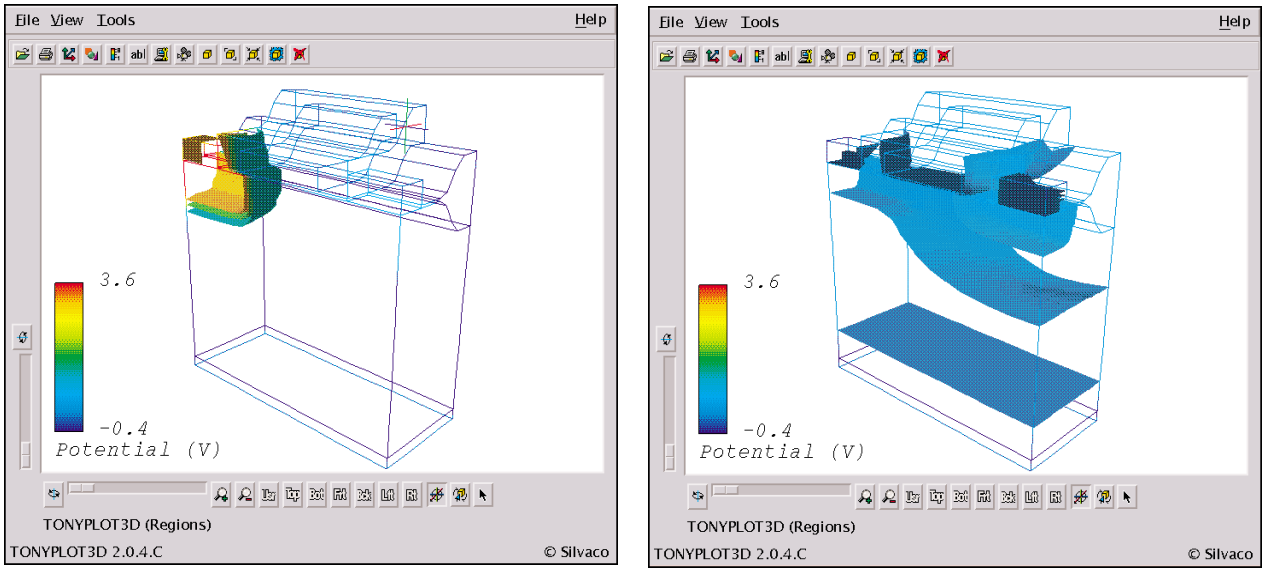

Figure 7. Potential Isosurfaces (a) Before SEU Strike (b) During SEU Strike When Electron-Hole Pair Generation is Near a Maximum.

Calendar of Events

February

1	
2	DesignCon '99 - Santa Clara
3	DesignCon '99 - Santa Clara
4	
5	
6	
7	
8	
9	
10	
11	
12	
13	
14	
15	
16	
17	ISSCC - San Francisco
18	ISSCC - San Francisco Analog '99 - Munich, Germany
19	Analog '99 - Munich, Germany
20	
21	
22	
23	
24	
25	
26	
27	
28	

March

1	
2	
3	
4	
5	
6	
7	
8	GOMAC - Monterey
9	GOMAC - Monterey DATE 99 - Munich, Germany
10	GOMAC - Monterey DATE 99 - Munich, Germany
11	GOMAC - Monterey DATE 99 - Munich, Germany
12	DATE 99 - Munich, Germany
13	
14	
15	
16	
17	
18	
19	
20	
21	
22	IRPS 99 - San Diego, CA
23	IRPS 99 - San Diego, CA
24	IRPS 99 - San Diego, CA
25	IRPS 99 - San Diego, CA
26	
27	
28	
29	
30	
31	

Bulletin Board

VWF 1999 Release Shipping in March!

The latest release of all the VWF products will begin shipping in March. This release includes new versions for ***ATLAS, ATHENA***, all the ***Interactive Tools*** and the ***Automation Tools***. All currently maintained TCAD users should receive a CD ROM and a totally reworked set of five users manuals.

See Silvaco Tools at GOMAC!

Silvaco International will be demonstrating at GOMAC '99. The conference will take place March 8-11 at the Hyatt Hotel in Monterey, CA. Silvaco continues to be a leading vendor at this important event.

Visit Silvaco at IRPS 99!

Look for a Silvaco booth to obtain the latest literature on all TCAD Driven CAD products and a demonstration at the International Reliability Physics Symposium in San Diego March 22-25. Silvaco staff will be on hand every day of the conference to highlight the new capabilities of the Silvaco tools.

If you would like more information or to register for one of our our workshops, please check our web site at ***http://www.silvaco.com***

The Simulation Standard, circulation 17,000 Vol. 10, No. 2, February 1999 is copyrighted by Silvaco International. If you, or someone you know wants a subscription to this free publication, please call (408) 567-1000 (USA), (44) (1483) 401-800 (UK), (81)(45) 341-7220 (Japan), or your nearest Silvaco distributor.

Simulation Standard, TCAD Driven CAD, Virtual Wafer Fab, Analog Alliance, Legacy, ATHENA, ATLAS, MERCURY, VICTORY, VYPER, ANALOG EXPRESS, RESILIENCE, DISCOVERY, CELEBRITY, Manufacturing Tools, Automation Tools, Interactive Tools, TonyPlot, TonyPlot3D, DeckBuild, DevEdit, DevEdit3D, Interpreter, ATHENA Interpreter, ATLAS Interpreter, Circuit Optimizer, MaskViews, PSTATS, SSuprem3, SSuprem4, Elite, Optolith, Flash, Silicides, MC Depo/Etch, MC Implant, S-Pisces, Blaze/Blaze3D, Device3D, TFT2D/3D, Ferro, SiGe, SiC, Laser, VCSELS, Quantum2D/3D, Luminous2D/3D, Giga2D/3D, MixedMode2D/3D, FastBlaze, FastLargeSignal, FastMixedMode, FastGiga, FastNoise, Mocasim, Spirit, Beacon, Frontier, Clarity, Zenith, Vision, Radiant, TwinSim, , UTMOST, UTMOST II, UTMOST III, UTMOST IV, PROMOST, SPAYN, UTMOST IV Measure, UTMOST IV Fit, UTMOST IV Spice Modeling, SmartStats, SDDL, SmartSpice, FastSpice, Twister, Blast, MixSim, SmartLib, TestChip, Promost-Rel, RelStats, RelLib, Harm, Ranger, Ranger3D Nomad, QUEST, EXACT, CLEVER, STELLAR, HIPEX-net, HIPEX-r, HIPEX-c, HIPEX-rc, HIPEX-crc, EM, Power, IR, SI, Timing, SN, Clock, Scholar, Expert, Savage, Scout, Dragon, Maverick, Guardian, Envoy, LISA, ExpertViews and SFLM are trademarks of Silvaco International.

Hints, Tips and Solutions

William French, Applications and Support Manager

Q: Can internal variables such as potential and current density be seen during 3D Resistance or Capacitance extraction in Clever.

A: ***Clever*** allows users to save a structure for each solution during a resistance or capacitance extraction. During capacitance extraction the solution is calculated inside the insulator materials. Values of electric field can be plotted throughout the insulator material to determine voltage drops.

For resistance analysis the potential, electric field and current density are calculated within each conductor. The distribution of field and current density can be useful to evaluate the effect of process variations such as lithographic thinning of metal lines or rounding of contacts.

To save 3D structures continuing these internal variables during a resistance calculation the syntax is:

```
INTERCONNECT RESISTANCE ADAPT=0.01\
                                    STRUCTURE="filename"
```

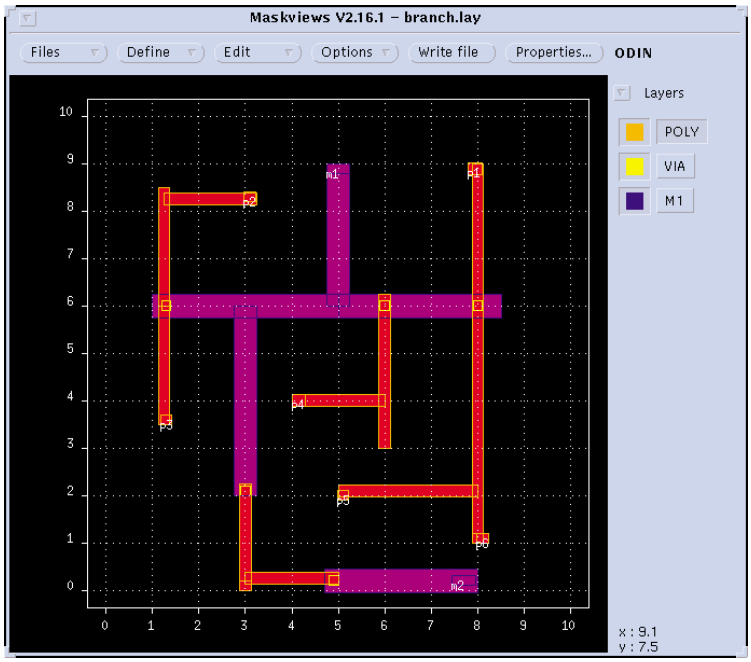

Figure 1. Layout of net within a cell. Combining this geometry with process information allows ***Clever*** to create a 3D structure of the conductors.

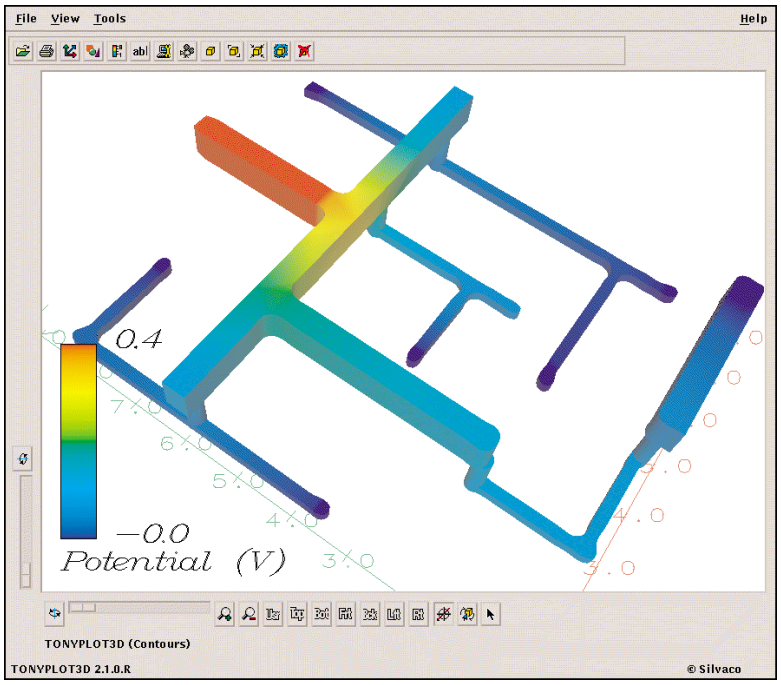

Figure 2. Potential distribution within the interconnect of the net.

ADAPT specifies the relative error to which the resistance is calculated. The mesh is automatically refined until this tolerance is met. The STRUCTURE parameter specifies the filename root for the 3D solution files. Since ***Clever*** solves separately for each resistance terminal there will be one file for every electrode defined in the structure. These files will be called filename.0.0, filename.0.1,filename.0.2 etc. A similar syntax exists for capacitance extraction.

Figure 1 shows the layout of the signal distribution in a cell. For clarity a single metal layer plus poly is considered. Figure 2 shows the potential distribution in this cell. Figure 3 shows the current density. The current is highest in the nearest poly track.

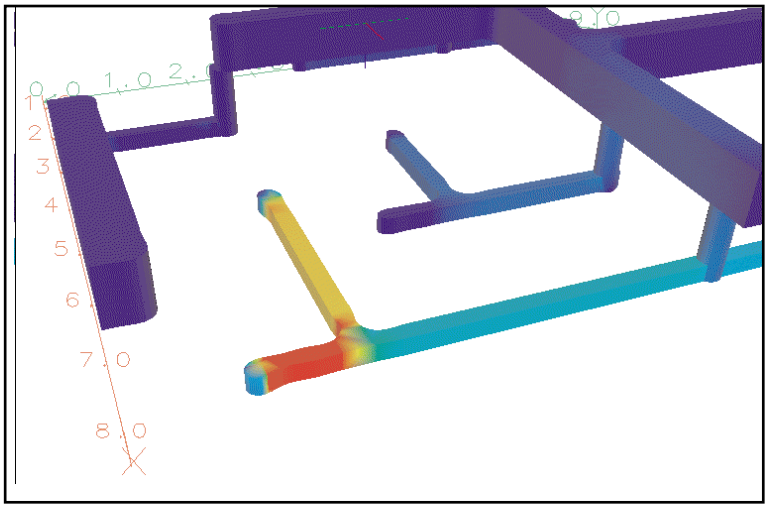

Figure 3. Current density in the interconnect. Note the lithographic geometry.

The CRITICAL parameter is used to determine which contour of the aerial image is taken to the etch location of the photoresist. Since the image value varies from zero to unity, CRITICAL should be in this range. A higher value of CRITICAL leads corresponds to over-exposed or over-developed image with thinner tracks, a lower value to under-exposed or under-developed image with thicker tracks. This simple parameter makes including lithography effects practical for users without the need for full 3D modeling of the exposure and development for the complete cell.

Q: When using lithography to accurately model deep-sub-micron features how can I view the image on the photoresist? How can I simply control the transfer of the image to the photoresist patterning?

Accurate extraction of resistance and capacitance for sub-0.5 micron designs requires the consideration of lithographic effects. ***Clever*** can model these effects using physical simulation of the optical or DUV lithography process.

The syntax used to specify lithography for a given layer is:

```
ILLUMINATION WAVELENGTH=DUV

MASK "POLY" LITHO IMAGE="filename" \
   CRITICAL=0.5
```

The ILLUMINATION statement specifies the wavelength of the stepper. Several other photolithography model parameters can also be specified covering the numerical aperture, filter, pupil and other factors. The LITHO parameter of the MASK statement is the key flag to enable the lithography modeling. The parameter IMAGE specifies a filename for saving the aerial image. This is a 2D file that can be viewed in ***TonyPlot***.

Figure 4 shows the aerial image from the polysilicon masking step for the layout in Figure 1. Corner rounding and line shortening are clearly seen. OPC techniques can be applied and will be described in a future *Simulation Standard* article.

Call for Questions

If you have hints, tips, solutions or questions to contribute, please contact our Applications and Support Department

Phone: (408) 567-1000 Fax: (408) 496-6080

e-mail: *support@silvaco.com*

Hints, Tips and Solutions Archive

Check our our Web Page to see more details of this example plus an archive of previous Hints, Tips, and Solutions

www.silvaco.com

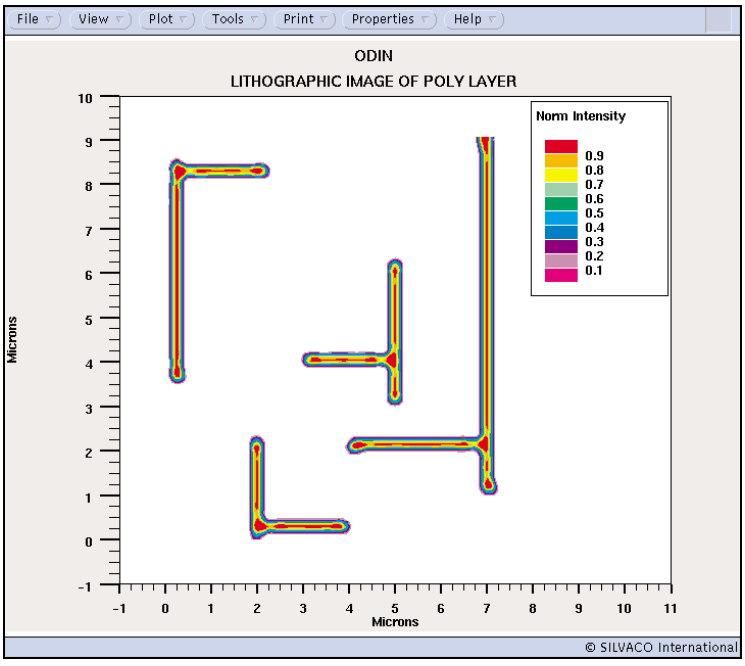

Figure 4. Optical image of the POLY layer from the layout in Figure 1.

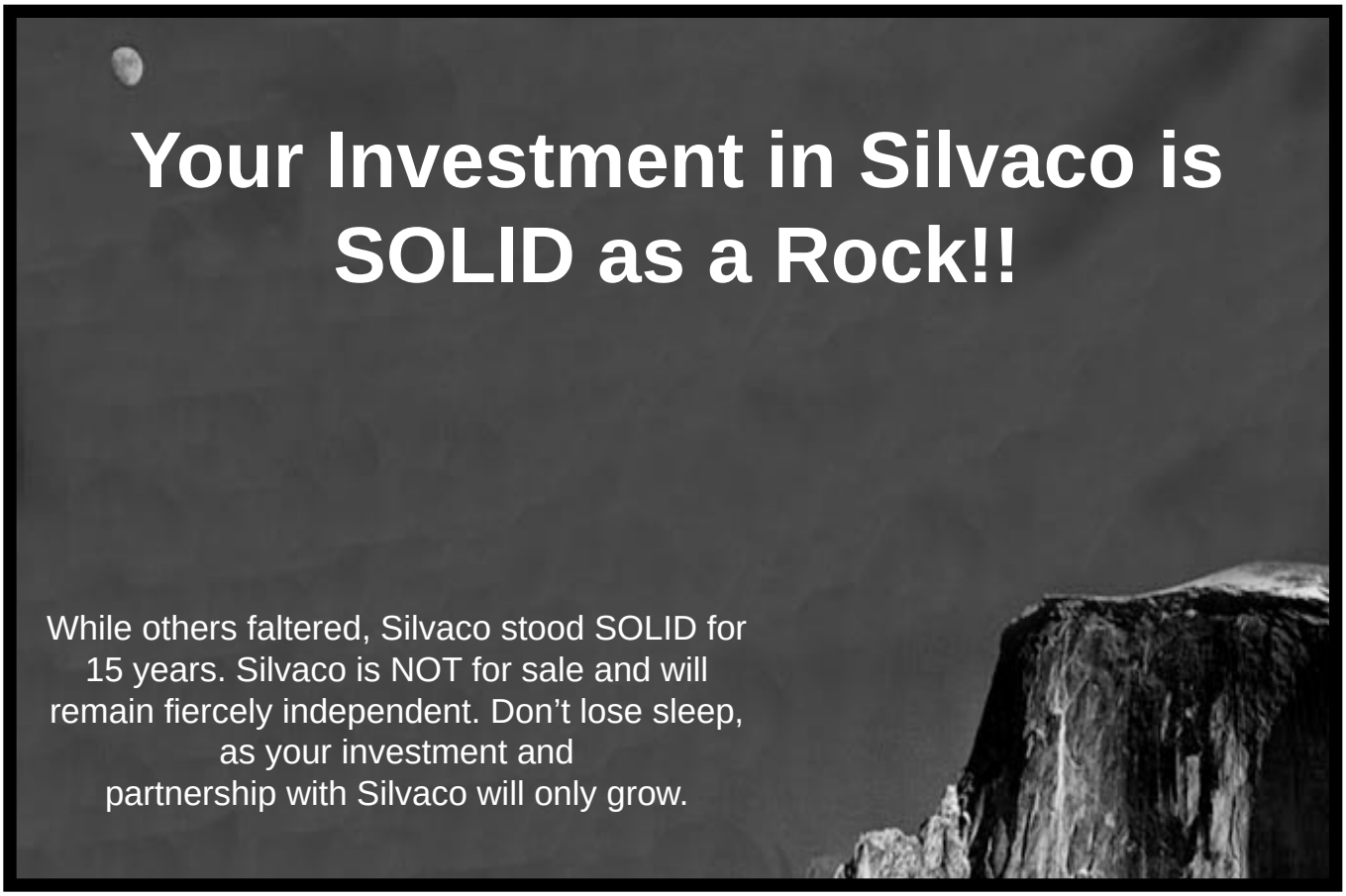

SILVACO
INTERNATIONAL

USA HEADQUARTERS

Silvaco International
4701 Patrick Henry Drive
Building 2
Santa Clara, CA 95054
USA

Phone: 408-567-1000
Fax: 408-496-6080

sales@silvaco.com
www.silvaco.com

CONTACTS:

Silvaco Japan
jpsales@silvaco.com

Silvaco Korea
krsales@silvaco.com

Silvaco Taiwan
twsales@silvaco.com

Silvaco Singapore
sgsales@silvaco.com

Silvaco UK
uksales@silvaco.com

Silvaco France
frsales@silvaco.com

Silvaco Germany
desales@silvaco.com

Products Licensed through Silvaco or e*ECAD

e*ECAD
Vendor Partner